Abdominal Radiology

Published online: 4 August 2018

Abdom Radiol (2019) 44:110–121
https://doi.org/10.1007/s00261-018-1727-5

Gadoxetic acid enhanced magnetic resonance imaging for prediction of the postoperative prognosis of intrahepatic mass-forming cholangiocarcinoma

Sungwon Kim,[1] Chansik An,[1] Kyunghwa Han,[1] and Myeong-Jin Kim[1]

[1]Department of Radiology and Research Institute of Radiological Science, Severance Hospital, Yonsei University College of Medicine, 50 Yonsei-ro, Shinchon-dong, Seodaemun-gu, Seoul 120-752, Republic of Korea

Abstract

Purpose: To identify imaging markers that independently predict the post-operative outcome of intrahepatic mass-forming cholangiocarcinoma (IMCC) using gadoxetate disodium-enhanced magnetic resonance imaging (MRI).

Methods: Data from 54 patients who underwent pre-operative gadoxetate disodium-enhanced MRI and curative surgery for IMCC were retrospectively evaluated. The prognostic power of various imaging and pathological features reportedly associated with recurrence-free survival (RFS) and overall survival (OS) was analyzed using Cox regression models. A model combining imaging and pathological features was developed and its performance was evaluated using the Harrell C-index and Akaike information criterion.

Results: Capsule penetration ($P = 0.016$) and tumor size ($P = 0.015$) were independent markers for worse RFS, while capsule penetration ($P = 0.012$) and hepatic vein obstruction (HVO, $P = 0.016$) were independent markers for worse OS, respectively, in the imaging-based model. Capsule penetration was the only imaging marker identified in the combined prediction model of RFS, and the combined model showed a higher C-index and lower AIC value compared with the model based on pathological features alone.

Conclusions: Capsule penetration and HVO on MRI are significantly worse imaging prognostic factors for post-operative outcomes in patients with IMCC. Incorporation of capsule penetration and HVO into a surgical staging system may improve prediction of the post-operative prognosis of IMCC.

Key words: Prognostic factors—Intrahepatic cholangiocarcinoma—Magnetic resonance imaging—Disodium gadoxetate

Abbreviations

ADC	Apparent diffusion coefficient
AIC	Akaike information criterion
AJCC	American Joint Committee on Cancer
AP	Arterial phase
AVI	Any vascular invasion
BDI	Bile duct invasion
BO	Biliary obstruction
CI	Confidence interval
CT	Computed tomography
DWI	Diffusion-weighted images
HBP	Hepatobiliary phase
HR	Hazard ratio
HVO	Hepatic vein obstruction
IMCC	Intrahepatic mass-forming cholangiocarcinoma
LCSGJ	Liver Cancer Study Group of Japan
MRI	Magnetic resonance imaging
MVI	Microvessel invasion
OS	Overall survival
PVO	Portal vein obstruction
RCS	Restricted cubic splines
RFS	Recurrence-free survival
SI	Signal intensity

Intrahepatic cholangiocarcinoma is the second most common primary malignant tumor of the liver [1]. Sur-

Electronic supplementary material The online version of this article (https://doi.org/10.1007/s00261-018-1727-5) contains supplementary material, which is available to authorized users.

Correspondence to: Myeong-Jin Kim; *email:* kimnex@yuhs.ac

gery is considered the only curative treatment for intrahepatic mass-forming cholangiocarcinoma (IMCC), although the 5-year survival rate is reported as 13%–42% even if curative surgery is attempted [2].

Various pathological markers have been adopted in surgical staging systems for the prediction of the prognosis of IMCC [3–6]. Among these, the recently developed 8th edition of the American Joint Committee on Cancer (AJCC) staging system [7] and a system proposed by the Liver Cancer Study Group of Japan (LCSGJ) are commonly used [3, 4].

Meanwhile, certain imaging features have been reported to be useful for the prediction of the prognosis of IMCC. These include hypervascular enhancement pattern on computed tomography (CT) as a sign of a favorable prognosis [8–10] and delayed enhancement on CT or magnetic resonance imaging (MRI) [11, 12]; intermediate signal intensity (SI) or target appearance on gadoxetate-enhanced hepatobiliary phase (HBP) images [13, 14]; and diffuse restriction in less than one-third of the tumor, which indicates abundant fibrous stoma, as signs of an unfavorable prognosis [15]. In unresectable intrahepatic cholangiocarcinoma, volume changes of ADC and viable tumors after locoregional treatment are known to be associated with prognosis [16]. However, the usefulness of combining imaging markers and the surgical staging system for better prediction of the post-operative outcome of IMCC remains unknown.

In the present study, we identified imaging markers that independently predict the post-operative outcome of IMCC using gadoxetate disodium-enhanced MRI and assessed whether using the identified imaging markers in conjunction with surgical pathological markers can improve prediction of the post-operative prognosis.

Materials and methods

Patient selection

Our institutional review board approved this retrospective study, and the requirement for informed consent was waived. After searching the electronic medical record database from January 2008 to January 2014, we identified 118 patients with intrahepatic cholangiocarcinoma who underwent curative hepatectomy. Patients with periductal infiltrative or intraductal growth types (n = 37) of cholangiocarcinoma, those who had not undergone preo-perative MRI (n = 16), and those with an interval of over 8 weeks between MRI and surgery (n = 11) were excluded. Eventually, 54 patients (mean age, 65 years; range, 36–80 years; 34 men and 20 women) who underwent gadoxetate disodium-enhanced MRI and did not undergo neoadjuvant treatment before surgery were included in the study (Fig 1). Five patients had liver cirrhosis and 12 had chronic hepatitis (Table 1), as confirmed by pathological examination, and all patients underwent curative R0 resection.

Image acquisition

MRI was performed using one of three 3.0-T systems (Magnetom Trio a Tim; Siemens Medical Solutions, Erlangen, Germany; Achieva, Philips Medical Systems, Best, the Netherlands; Discovery, GE Medical Systems, Milwaukee, Wisconsin, USA) or a 1.5-T system (Achieva 1.5-T, Philips Medical Systems).

All images were obtained in the transverse plane with a field of view of 44 × 33 cm or 40 × 30 cm. First, two-dimensional dual-echo T1-weighted gradient-recalled-echo images were obtained (in-phase and opposed-phase). Dynamic images were obtained before and after

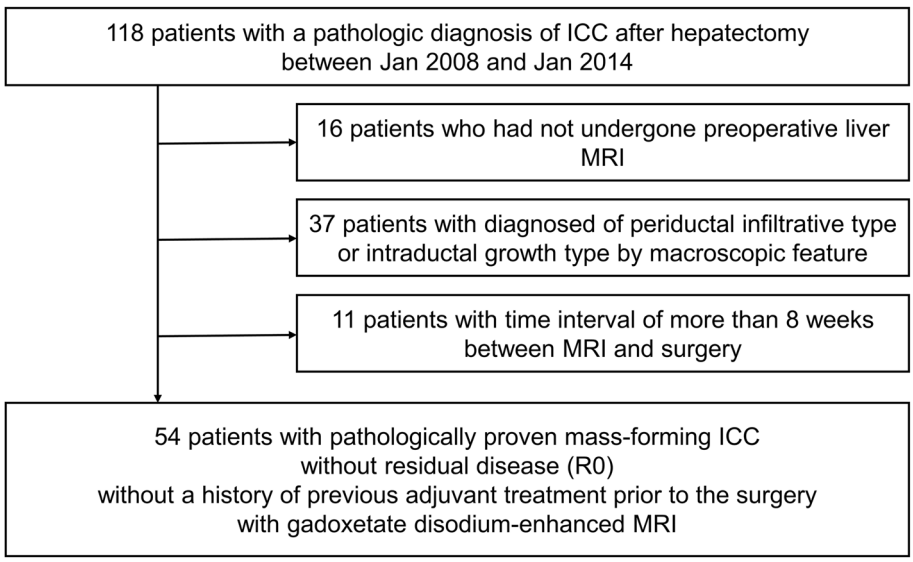

Fig. 1. Flow chart showing the inclusion and exclusion criteria for our study.

Table 1. Characteristics of patients with intrahepatic mass-forming cholangiocarcinoma included in the study

Variables	Values
Ages (year), mean ± SD (range)	65 ± 11 (36–80)
Sex, male:female (%)	34:20 (63:37)
Underlying liver disease, present:absent (%)	17 (31.5):37 (68.5)
Liver cirrhosis (hepatitis B)[a]	4 (23.5)
Liver cirrhosis (alcoholic)[a]	1 (5.9)
Chronic hepatitis B	3 (17.6)
Chronic hepatitis C	1 (5.9)
Alcoholic hepatitis	4 (23.5)
Non-alcoholic fatty liver disease	2 (11.8)
Unknown cause	2 (11.8)
Post-operative treatment (%)	24 (44.4)
Chemotherapy	20 (83)
Radiotherapy	3 (13)
Combined chemoradiotherapy	1 (4)
Tumor size (cm)	4.7 (2.0)

SD, standard deviation
[a]Cirrhosis was classified as Child-Pugh class A in all affected patients

contrast material administration in arterial, portal venous, hepatic venous, and final dynamic phases by using a T1-weighted three-dimensional gradient-echo sequence (Table 2). To determine the imaging delay for arterial phase imaging, a bolus technique was used with 1 mL of gadoxetic acid disodium (Primovist; Bayer Schering Pharma, Berlin, Germany) and a 20 mL 0.9% saline chaser at an injection rate of 1 or 2 mL/s to determine the peak enhancement of the abdominal aorta. For dynamic imaging, 0.1 mL/kg (0.025 mmol/kg) of gadoxetic acid disodium was injected, followed by a 20 mL saline chaser at the same rate as that used for the bolus injection. T2-weighted images were obtained with multi-shot and single-shot turbo spin-echo sequences by using a navigator-triggered technique. Diffusion-weighted images (DWI) were also obtained by using a navigator-triggered technique at b values of 50, 400, and 800 s/mm^2, and the apparent diffusion coefficient (ADC) was calculated by the MR units.

Image analysis and pathological evaluation

All MR images were retrospectively and independently reviewed on a picture acquisition and communication system workstation (Centricity 4.0, GE Healthcare, Milwaukee, WI, USA) by two radiologists with 25 and 3 years of experience in abdominal imaging, respectively. Both radiologists were aware of the diagnosis of IMCC but were blinded to the pathological details. They independently performed the image analysis, and any disagreement was resolved by consensus. The interobserver agreement was assessed before arriving at a consensus.

The MR images were qualitatively analyzed for the following features: tumor size, tumor number, arterial phase (AP) enhancement pattern, peritumoral enhancement, infiltrative margin, SI pattern on HBP images, hypointense rim on HBP images, target appearance on DWI, biliary obstruction (BO), portal vein obstruction (PVO), hepatic vein obstruction (HVO), tumor extension to the capsule, capsule penetration by the tumor, lymph node metastasis, and liver parenchymal atrophy. The AP enhancement pattern was classified into three categories according to a recent study [8]: hypervascular, rim-enhanced, and hypovascular. The SI pattern on HBP images was classified into two groups [13, 14]: an intermediate group, defined as the presence of a hyper- or isointense area (relative to the spleen) occupying ≥ 50% of the tumor, and a hypointense group, defined as the presence of a hyper- or iso-intense area occupying < 50% of the tumor [13]. According to the ratio of the diffusion-restricted area to the tumor area, tumors were categorized into Group 1 when the ratio was < 1/3 and Group 2 when the ratio was > 1/3 [15]. BO, PO, and HVO were diagnosed when definite obstructions were observed on the images. Capsule extension was defined when the tumor abutted on Glisson's capsule, and capsule penetration was defined when the tumor extruded outside Glisson's capsule. Parenchymal atrophy was diagnosed when parenchymal volume loss was noted around the tumor.

The surgical specimens of all patients were subjected to histopathological analysis; we retrieved the pathology reports from the electronic medical record system for surgical specimens at our hospital. All identified pathological features are listed in Table 3.

Evaluation of outcomes

All patients underwent contrast-enhanced CT or MRI at 3–6 months after surgery and were followed up for 2.3–96.7 months (mean 35.0 months). During the follow-up period, we retrospectively reviewed the medical records for tumor recurrence, presence and type of adjuvant treatment, and survival period. Tumor recurrence was determined by combining follow-up CT or MRI, and clinical findings. Recurrence-free survival (RFS) was defined as the interval between the date of surgery and the first date of tumor recurrence on imaging or the last follow-up date without recurrence, and overall survival (OS) was defined as the interval between the date of surgery and the date of patient death or the last follow-up without death.

Statistical analysis

RFS and OS were assessed by the Kaplan–Meier method, and differences in survival distributions between groups were compared using log-rank tests. Multivariate Cox regression analysis was performed for variables with a P value of ≤ 0.2 in the univariate Cox regression analysis. A backward stepwise selection based on the Akaike information criterion (AIC) was used to prepare

Table 2. Magnetic resonance image acquisition parameters for patients with intrahepatic mass-forming cholangiocarcinoma

Acquisition sequence	Scanner trade name (field strength)	Matrix size	Section thickness (mm)	Intersection gap (mm)	Repetition time (ms)	Echo time (ms)	Flip angle (°)
Dual-echo T1-weighted gradient-recalled-echo	Magnetom Trio Tim (3 T)	256 × 192	3	0.6	4	2.46 and 1.23	9
	Intera Achieva (3 T)	160 × 160	5	1	219	2.3 and 1.1	20
	Intera Achieva (1.5 T)	288 × 231	7	0.7	189	4.6 and 2.3	80
	Discovery MR750w (3 T)	320 × 250	4	1	4.9	2.3 and 1.1	10
T1-weighted 3D gradient-echo with dynamic contrast enhancement[a]	Magnetom Trio Tim (3 T)	256 × 192	2	0.4	2.54	0.95	13
	Intera Achieva (3 T)	256 × 220	2	0	3	1.42	10
	Intera Achieva (1.5 T)	256 × 166	4	0	4.2	2.0	10
	Discovery MR750w (3 T)	224 × 192	2.5	0	190	1.2–4.7	10
T2-weighted turbo spin-echo, navigator-triggered	Magnetom Trio Tim (3 T)	320 × 168	2	0.4	2.54	0.95	140
	Intera Achieva (3 T)	288 × 192	5	1	988	80	90
	Intera Achieva (1.5 T)	288 × 228	7	0	452	80	90
	Discovery MR750w (3 T)	320 × 320	4	1	4286	73	15
Diffusion-weighted imaging	Magnetom Trio Tim (3 T)	128 × 96	5	1	5200	67	90
	Intera Achieva (3 T)	288 × 192	5	1	8500	57	90
	Intera Achieva (1.5 T)	112 × 144	7	1	1600	62	90
	Discovery MR750w (3 T)	96 × 128	4	1	5800	62	90

[a]The arterial phase began 2 or 3 s after the peak aortic enhancement was determined with the bolus injection; subsequent dynamic images were obtained at intervals of approximately 30 s. Each dynamic image acquisition required 18–24 s. Hepatobiliary images were obtained 15 or 20 min after injection of the contrast material by using the same imaging sequence as that used for the pre- and postcontrast images

a multivariate prediction model. Hazard ratios (HRs) and 95% confidence intervals (CIs) were measured. Continuous variables with nonlinearity were transformed using restricted cubic splines (RCS) transformation to maximize the Wald chi-square statistic and transformed to linear splines for intuitive analysis (Online Resource 1). The performance comparison between models was aimed at identifying a model that minimizes the AIC value while maximizing the Harrell C-index. The interobserver agreement for imaging features was measured using simple unweighted Cohen kappa statistics [17]. The agreement was rated on the following scale: k = 0–0.20, slight agreement; 0.21–0.40, fair agreement; 0.41–0.60, moderate agreement; 0.61–0.80, substantial agreement; and ≥ 0.81, excellent agreement [18]. All statistical analyses were performed using the R software (version 3.3.1, R Foundation for Statistical Computing, Vienna, Austria). A P value of < 0.05 was considered statistically significant.

Results

Pathological and imaging feature analysis for RFS

With regard to the pathological features, univariate analysis revealed that tumor size, tumor multiplicity, macroscopic bile duct invasion (BDI), microvessel invasion (MVI), any vascular invasion (AVI), adjacent organ invasion, and lymph node metastasis were significant markers of RFS (Table 3, Fig 2). Multivariate analysis revealed that tumor multiplicity ($P < 0.001$), macroscopic BDI ($P = 0.020$), MVI ($P = 0.005$), and adjacent organ invasion ($P = 0.004$) were independent markers of RFS (Table 3).

With regard to the imaging features, tumor size was the only significant marker of RFS in the univariate analysis. However, infiltrative margin, BO, and capsule penetration were close to significance (Table 3) and showed significant differences in the survival analysis (Fig. 2). In multivariate analysis, tumor size ($P = 0.015$) and capsule penetration ($P = 0.016$) were independent factors for RFS (Table 3, Figs. 3, 4).

The interobserver agreement was excellent for BO; substantial for parenchymal atrophy, capsule penetration, AP enhancement pattern, multiplicity, and lymph node metastasis; moderate for PVO, HVO, hypointense rim on HBP, infiltrative margin, capsule extension, and DWI pattern; and fair for the remaining features (Table 3).

Model with combined pathological and imaging features for RFS

When both pathological and imaging features were considered together, multiplicity ($P < 0.001$), macroscopic BDI ($P = 0.011$), MVI ($P = 0.006$), and adjacent organ invasion ($P < 0.001$) were found to be independent pathological markers, while capsule penetration ($P = 0.044$) was the only imaging marker (Table 3). A new combined model derived from these markers showed a higher C-index (0.799 vs. 0.795) and lower AIC value (155.1 vs. 155.9) compared with the model based on pathological features alone.

Pathological and imaging feature analysis for OS

For the prediction of OS, the univariate analysis revealed that macroscopic BDI, microscopic BDI, MVI, and AVI

Table 3. Findings of univariate and multivariate cox analyses for pathological, imaging, and combined models for the prediction of recurrence-free survival in patients with intrahepatic mass-forming cholangiocarcinoma

Pathologic features		Univariate			Multivariate		
		HR	95% CI	*P* Value	HR	95% CI	*P* Value
Size		1.30	1.06, 1.60	0.011*			
Multiplicity		4.18	1.70, 10.32	0.002*	7.06	2.51, 19.90	< 0.001*
Macroscopic bile duct invasion		2.34	1.06, 5.18	0.036*	2.85	1.18, 6.90	0.020*
Microscopic bile duct invasion		1.41	0.65, 3.08	0.386			
Portal vein invasion		2.00	0.75, 5.34	0.165			
Hepatic vein invasion		NA	NA	NA			
Hepatic artery invasion		NA	NA	NA			
Microvessel invasion		4.79	1.43, 16.02	0.011*	6.09	1.71, 21.71	0.005*
Any vascular invasion		3.87	1.16, 12.92	0.028*			
Serosal invasion		0.72	0.30, 1.73	0.467			
Adjacent organ invasion		3.66	1.25, 10.75	0.018*	6.95	1.86, 25.99	0.004*
Lymph node metastasis		2.49	1.07, 5.82	0.035*	2.09	0.81, 5.40	0.129
Tumor necrosis		1.55	0.71, 3.37	0.268			
Differentiation							
Moderate (vs. Well)		0.94	0.12, 7.50	0.950			
Poor (vs. Well)		3.41	0.45, 26.11	0.237			
Age		1.02	0.98, 1.06	0.430			
Cirrhosis		0.70	0.17, 2.98	0.632			
Adjuvant treatment		2.01	0.92, 4.41	0.080			
MRI imaging features	κ	HR	95% CI	*P* Value	HR	95% CI	*P* Value
Size	N/A	1.32	1.07, 1.63	0.011*	1.39	1.07, 1.81	0.015*
Multiplicity	0.71	0.93	0.28, 3.09	0.899			
Arterial enhancement pattern	0.71						
Hypervascular (vs. rim)		1.10	0.45, 2.65	0.837			
Hypovascular (vs. rim)		1.90	0.67, 5.36	0.225			
Peritumoral enhancement	0.39	1.71	0.64, 4.54	0.284			
Infiltrative margin	0.51	2.35	0.98, 5.63	0.055	2.13	0.89, 5.11	0.090
HBP SI pattern (intermediate vs. hypointense)	0.26	1.52	0.66, 3.51	0.323			
HBP hypointense rim	0.51	0.61	0.28, 1.33	0.211			
DWI pattern (Group 1 vs. Group 2)	0.44	1.26	0.52, 3.08	0.610			
Biliary obstruction	0.85	2.35	0.98, 5.62	0.056	2.17	0.86, 5.46	0.101
Portal vein obstruction	0.56	1.39	0.64, 3.02	0.410			
Hepatic vein obstruction	0.55	3.01	0.87, 10.49	0.083	2.94	0.79, 10.92	0.108
Capsule penetration	0.73	4.02	0.90, 17.92	0.068	7.02	1.43, 34.45	0.016*
Capsule extension	0.47	1.21	0.56, 2.65	0.628			
Lymph node metastasis	0.61	1.64	0.75, 3.61	0.217			
Atrophy	0.74	1.53	0.46, 5.13	0.490			
Combined pathologic and imaging model							
Multiplicity					6.98	2.55, 19.11	< 0.001*
Macroscopic bile duct invasion					3.08	1.29, 7.36	0.011*
Microvessel invasion					5.59	1.63, 19.25	0.006*
Adjacent organ invasion					9.20	2.60, 32.57	< 0.001*
Capsule penetration[a]					5.08	1.04, 24.73	0.044*

HR, hazard ratio; CI, confidence interval
[a]The only imaging feature included in the combined model
*Statistically significant results from Cox regression analysis

were significant markers (Table 4, Fig 5). Tumor size had a nonlinear effect on HR for OS. Therefore, linear spline transformation was applied to the tumor size using the minimal and maximal points (3.5, 6.5 cm) of the log relative hazard plot of the RCS transformation (Online Resource 1). In the multivariate analysis, tumor size ranging from 3.5 to 6.5 cm ($P = 0.018$), MVI ($P = 0.034$), and age ($P = 0.008$) were independent markers of poor OS (Table 4). The effect of tumor size on the risk of death showed a linear increase in the size range of 3.5–6.5 cm, following which the risk of death reached a plateau (Online Resource 1). The effect of tumor size on the risk of death did not show a linear increase or a statistically significant decrease for tumors measuring < 3.5 cm.

With regard to imaging features, HVO and capsule penetration were significantly poor markers of OS, whereas BO and LN metastasis were close to significance (Table 4) and showed a significant difference in the survival analysis (Fig. 5). In the multivariate analysis, HVO ($P = 0.016$) and capsule penetration ($P = 0.012$) were independent factors for OS (Table 4, Fig. 6).

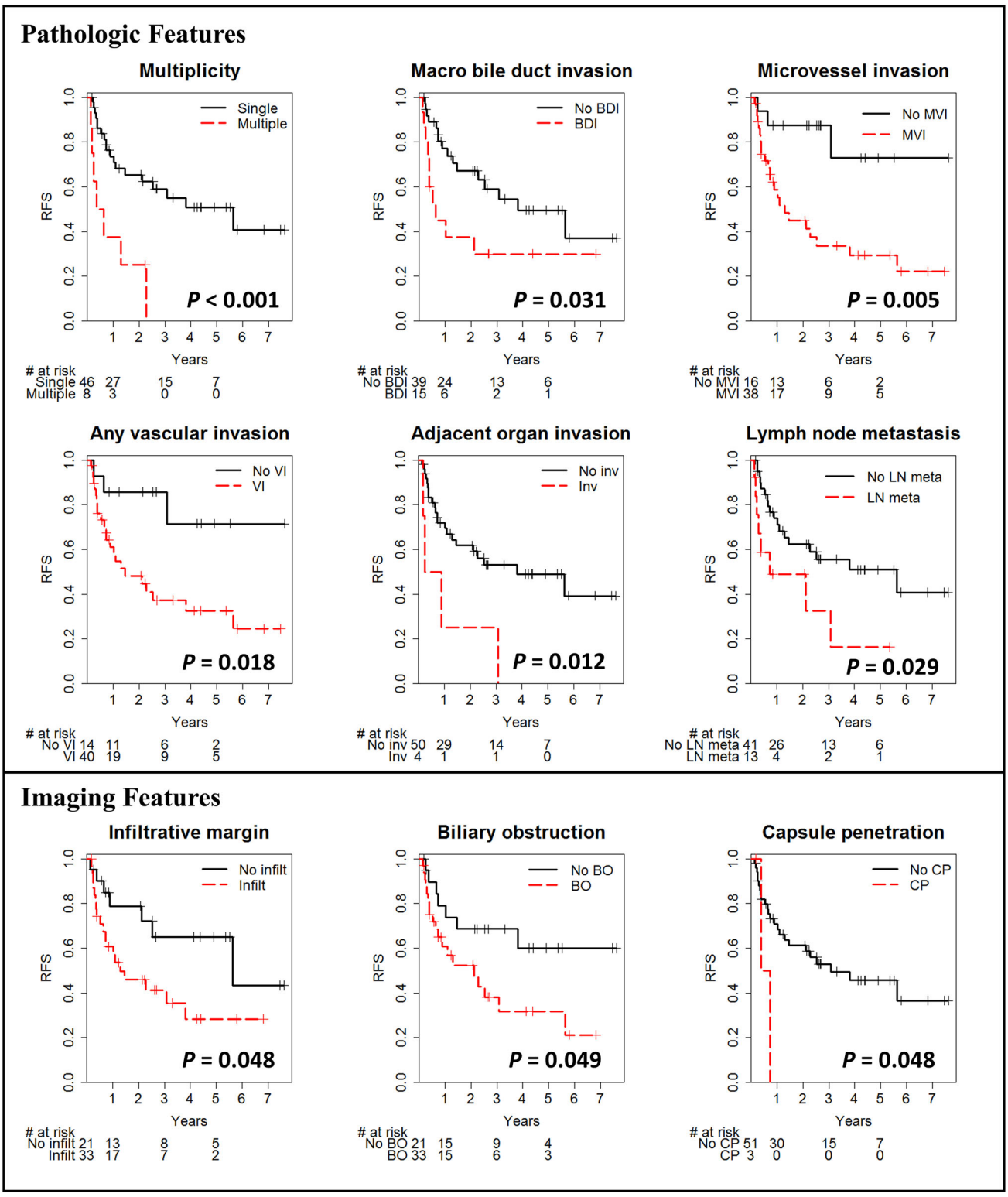

Fig. 2. Kaplan–Meier curves for RFS in patients with intrahepatic mass-forming cholangiocarcinoma exhibiting different pathological and imaging features. RFS is significantly poorer for patients with tumor multiplicity, macroscopic BDI, MVI, AVI, adjacent organ invasion, or lymph node metastasis than for those without these pathological features. In addition, RFS is significantly poorer for patients with infiltrative margins, BO, or capsule penetration than for those without these features on magnetic resonance imaging. *P* values were calculated using log-rank tests. Continuous variables-tumor size was not plotted. RFS, recurrence-free survival; BDI, bile duct invasion; MVI, microvessel invasion; AVI, any vascular invasion; LN, lymph node; BO, biliary obstruction; CP, capsule penetration.

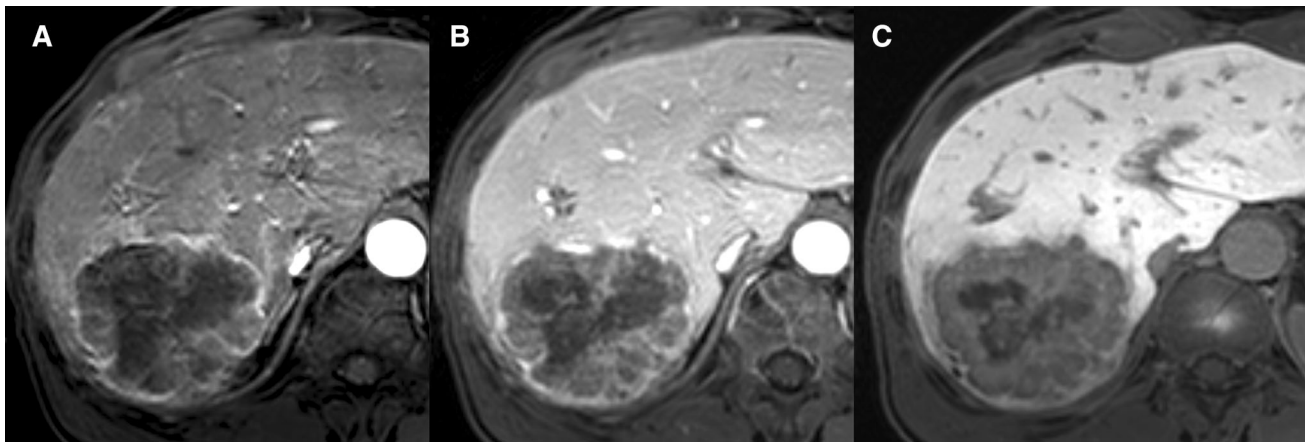

Fig. 3. Magnetic resonance imaging findings for a representative case involving a 67-year-old man exhibiting 7.5-cm size mass-forming intrahepatic cholangiocarcinoma. Axial fat-suppressed T1-weighted three-dimensional gradient-recalled echo images were obtained during the **A** arterial phase, **B** portal venous phase, and **C** hepatobiliary phase. The tumor exhibited a poor prognosis. The tumor recurred 8 months after the resection and the patient survived for only 10 months.

Model with combined pathological and imaging features for OS

When both pathological and imaging markers were considered together, no additional independent imaging marker was identified in addition to the pathological markers.

Review of pre-existing staging systems with the identified imaging predictors

When we compared the prognoses according to T-staging in the AJCC 6th, 7th, and 8th editions and the LCSGJ system with our data, we found that both the AJCC 6th and 7th editions showed insufficient prognostic predictions (Online Resource 1). The AJCC 8th edition showed better prognostic prediction, although the prognosis of the T3 stage was better than that of the T2 stage. The LCSGJ model showed the best order and separation among the T-staging curves. However, the separation of T3 and T4 curves with regard to OS was not adequate. Thus, we developed a new staging system by adding the two independent imaging markers for OS—capsule penetration and HVO—to the LCSGJ staging system. This new model featured capsule penetration or HVO on MRI as an additional criterion to designate the T4 stage. The new model showed better prognostic prediction, particularly in the separation between the T3 and T4 stages ($P = 0.010$ and 0.015; log-rank; Fig. 7). In addition, the C-index value for this new model was higher than those for all other models except the AJCC 8th edition (RFS; new model vs. 6th, 7th, and 8th AJCC and LCSGJ: 0.724 vs. 0.681, 0.662, 0.734, and 0.699, respectively; OS; new model vs. 6th, 7th, and 8th AJCC and LCSGJ: 0.720 vs. 0.664, 0.658, 0.671, and 0.646, respectively).

Discussion

In the present study, we identified imaging markers that independently predict the post-operative outcome of IMCC using gadoxetate disodium-enhanced MRI not only in the imaging prediction model but also in the combined imaging-pathological model. Our results showed that capsule penetration and tumor size were independent markers of RFS and capsule penetration and HVO were independent markers of OS in the imaging-based prognostic model for IMCC after resection. In the evaluation of a combined model including imaging and pathological findings, capsule penetration was the only independent imaging marker for RFS, while no imaging feature was identified as an independent marker for OS.

Imaging-defined capsule penetration may correspond to pathologically defined serosal perforation or invasion, which is a poor prognostic factor that designates the T4 stage in the AJCC 6th edition and the T3 stage in the AJCC 7th and 8th editions. Interestingly, however, in the present study, capsule penetration observed on MRI showed a higher prognostic value compared with pathologically determined serosal invasion, particularly with regard to the prediction of RFS. This suggests that gross capsule penetration on MRI is associated with a higher prognostic value compared with microscopic penetration, and in-vivo analysis with inspection of the entire tumor area on MRI may reflect the significance of capsular penetration more accurately than the microscopic examination of excised specimens.

HVO has been reported as a poor prognostic factor [19], and many staging systems including the AJCC and LCSGJ staging systems (1st–5th editions) have adopted HVO as a prognostic factor in terms of vascular invasion [3, 6, 20]. However, HVO has been excluded from the

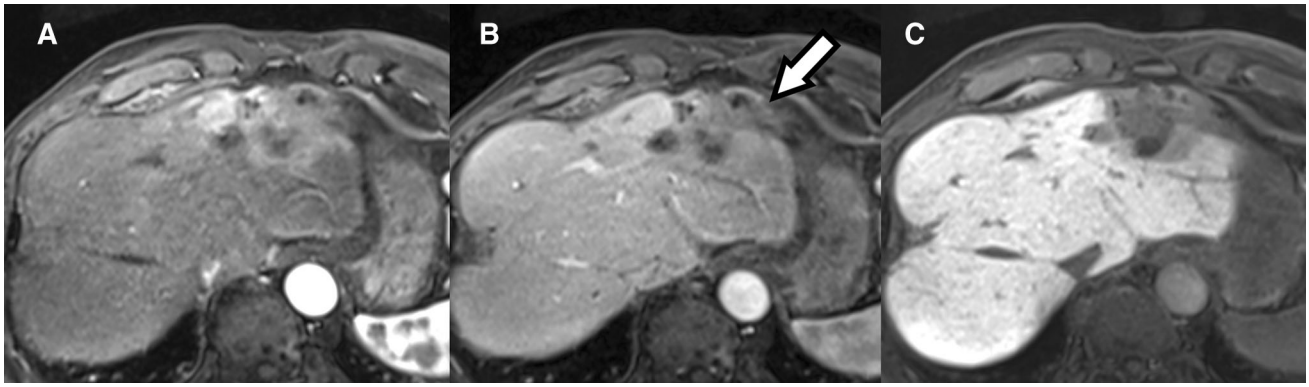

Fig. 4. Magnetic resonance imaging findings for a representative case involving a 67 year-old man exhibiting mass-forming intrahepatic cholangiocarcinoma with capsule penetration (arrow). Axial fat-suppressed T1-weighted three-dimensional gradient-recalled echo images obtained during the **A** arterial phase, **B** portal venous phase, and **C** hepatobiliary phase. The tumor exhibited a poor prognosis and recurred 4.5 months after resection. The patient survived for 19 months.

recent LCSGJ system proposed in 2016 because of its insufficient prognostic significance [4]. In the present study, HVO was identified as an independent marker of OS in the imaging-based model, although not in the combined model. Interestingly, the number of patients with HVO on MRI was higher than the number of patients with pathological hepatic vein invasion (5 vs. 1) in the present study; this implies that gross hepatic vein invasion or severe compression on MRI may be better associated with a poor prognosis compared with histological findings.

The best surgical staging model tested with our data for the prediction of post-operative outcomes was the recent LCSGJ model. The predictive power of the LCSGJ model seemed to be improved by adding the features of capsule penetration and HVO, which were identified as independent markers in the imaging-based model for OS. This may indicate that the imaging predictors derived from the present study can be well incorporated in the pre-existing surgical staging systems. The comparison of prognostic performances among the different staging systems was performed to demonstrate that when combined with the surgical staging system, the significant prognostic factors observed in imaging were also important in improving the prognostic performance. Though the large multicenter studies need to be conducted in the future, the imaging prognostic factors may help to improve the prognostic performance of the AJCC staging system as well as LCSGJ.

In the present study, previously reported imaging markers for prognosis, including the AP enhancement pattern, DWI pattern, and SI pattern on HBP images, were not identified as independent prognostic factors, possibly because the influence of imaging markers on the prognosis can be statistically underestimated in a small number of subjects, considering the prognostic power of pathological features is relatively high. In addition, the low interobserver agreement for the evaluation of some of the imaging features may have affected the result for the SI pattern on HBP images ($\kappa = 0.259$) and the DWI pattern ($\kappa = 0.440$). Therefore, further validation of the significance of imaging features as prognostic markers for IMCC after resection is necessary.

Tumor size linearly affected the risk of death in the size range of 3.5 to 6.5 cm, following which the risk of death reached a plateau (Online Resource 1). This result is similar to that in an international multicenter study reporting that tumor size linearly affects the risk of death up to 7 cm, following which it results in a plateau [3]. A threshold effect of tumor size is noted for many other tumors and forms the basis for various cut-off values for tumors in the AJCC TNM classification [6]. In addition, the effect of tumor size on the risk of death was not linear when the tumor measured < 3.5 cm in the present study, possibly because the number of patients was inadequate to show a significant correlation and because tumors measuring < 3.5 cm may show a similar post-operative prognosis.

Adjuvant treatment was not a significant prognostic factor in the present study. However, patients who received adjuvant treatment tended to show a poor prognosis, probably because adjuvant treatment was administered to patients with higher-stage lesions or suspected lymph node metastasis.

In the present study, the significant prognostic factors for RFS were more similar to those in the existing AJCC and LCSGJ staging systems. Although OS is an important endpoint to determine significant prognostic factors, it can differ because of various factors not related to the disease itself. Therefore, the identification of prognostic factors associated with RFS is of clinical importance [21].

This study has some limitations: First, because of the small sample size, it is possible that statistically signifi-

Table 4. Findings of univariate and multivariate cox analysis for pathological, imaging, and combined models for the prediction of overall survival in patients with intrahepatic mass-forming cholangiocarcinoma

Pathologic features	Univariate			Multivariate		
	HR	95% CI	*P* value	HR	95% CI	*P* value
Size (< 3.5 cm)	0.73	0.28, 1.87	0.508	0.36	0.12, 1.09	0.072
Size (≥ 3.5 and < 6.5 cm)	2.47	0.70, 8.65	0.158	5.93	1.37, 25.78	0.018*
Size (≥ 6.5 cm)	0.41	0.17, 1.00	0.051	0.43	0.14, 1.34	0.145
Multiplicity	1.97	0.65, 5.92	0.229			
Macroscopic bile duct invasion	2.39	1.02, 5.60	0.045*	2.28	0.93, 5.58	0.071
Microscopic bile duct invasion	2.53	1.07, 6.00	0.036*			
Portal vein invasion	0.98	0.29, 3.31	0.972			
Hepatic vein invasion	NA	NA	NA			
Hepatic artery invasion	NA	NA	NA			
Microvessel invasion	5.64	1.32, 24.07	0.020*	4.93	1.12, 21.57	0.034*
Any vascular invasion	4.73	1.11, 20.21	0.036*			
Serosal invasion	0.56	0.21, 1.52	0.257			
Adjacent organ invasion	1.26	0.30, 5.40	0.753			
Lymph node metastasis	2.11	0.86, 5.16	0.103			
Tumor necrosis	1.03	0.45, 2.38	0.945			
Differentiation						
Moderate (vs. Well)	1.36	0.18, 10.55	0.768			
Poor (vs. well)	1.91	0.24, 14.93	0.538			
Age	1.04	1.00, 1.09	0.082	1.08	1.02, 1.15	0.008*
Cirrhosis	0.42	0.06, 3.11	0.394			
Adjuvant treatment	2.03	0.88, 4.70	0.123	2.02	0.76, 5.37	0.158
MRI imaging features						
Size	1.14	0.96, 1.36	0.137			
Multiplicity	0.36	0.05, 2.71	0.324			
Arterial enhancement pattern						
Hypervascular (vs. rim)	0.90	0.36, 2.24	0.824			
Hypovascular (vs. rim)	0.76	0.17, 3.37	0.720			
Peritumoral enhancement	1.88	0.64, 5.53	0.252			
Infiltrative margin	1.40	0.60, 3.24	0.438			
HBP SI pattern (intermediate vs. hypointense)	0.71	0.31, 1.60	0.405			
HBP hypointense rim	0.50	0.22, 1.14	0.100			
DWI pattern (Group 1 vs. Group 2)	1.49	0.57, 3.90	0.418			
Biliary obstruction	2.49	0.98, 6.35	0.056	2.04	0.77, 5.40	0.151
Portal vein obstruction	1.26	0.55, 2.90	0.580			
Hepatic vein obstruction	4.92	1.50, 16.14	< 0.008*	4.72	1.33, 16.78	0.016*
Capsule penetration	5.64	1.23, 25.93	0.026*	7.63	1.56, 37.46	0.012*
Capsule extension	1.02	0.45, 2.31	0.963			
Lymph node metastasis	2.26	0.99, 5.13	0.052			
Atrophy	0.69	0.09, 5.14	0.713			
Combined pathologic and imaging model[a]						
Size (< 3.5 cm)				0.36	0.12, 1.09	0.072
Size (≥ 3.5 and < 6.5 cm)				5.93	1.37, 25.78	0.018*
Size (≥ 6.5 cm)				0.43	0.14, 1.34	0.145
Macroscopic bile duct invasion				2.28	0.93, 5.58	0.071
Microvessel invasion				4.93	1.12, 21.57	0.034*
Age				1.08	1.02, 1.15	0.008*
Adjuvant treatment				2.02	0.76, 5.37	0.158

HR, hazard ratio; CI, confidence interval
[a]Same as the pathological model without an independent imaging feature
*Statistically significant results from Cox regression analysis

cant variables were underestimated in our statistical analysis. However, the number of subjects in our study is not smaller than that in most previous studies evaluating the relationship between imaging features and post-operative outcomes [8, 9, 11, 13]. Second, our study did not reflect the prognosis of lymph node metastasis or distant metastasis corresponding to NM staging because all patients underwent curative R0 resection. Lymph node metastases in all patients were resectable, regional metastases. Third, because of the long study period of over 5 years, diverse MR systems were used. However, this may also increase the possibility of generalization of our results.

In conclusion, the results of the present study suggest that capsule penetration and HVO on MRI are significantly worse imaging prognostic factors for post-operative outcomes in patients with IMCC. Incorporation of capsule penetration and HVO into a surgical staging

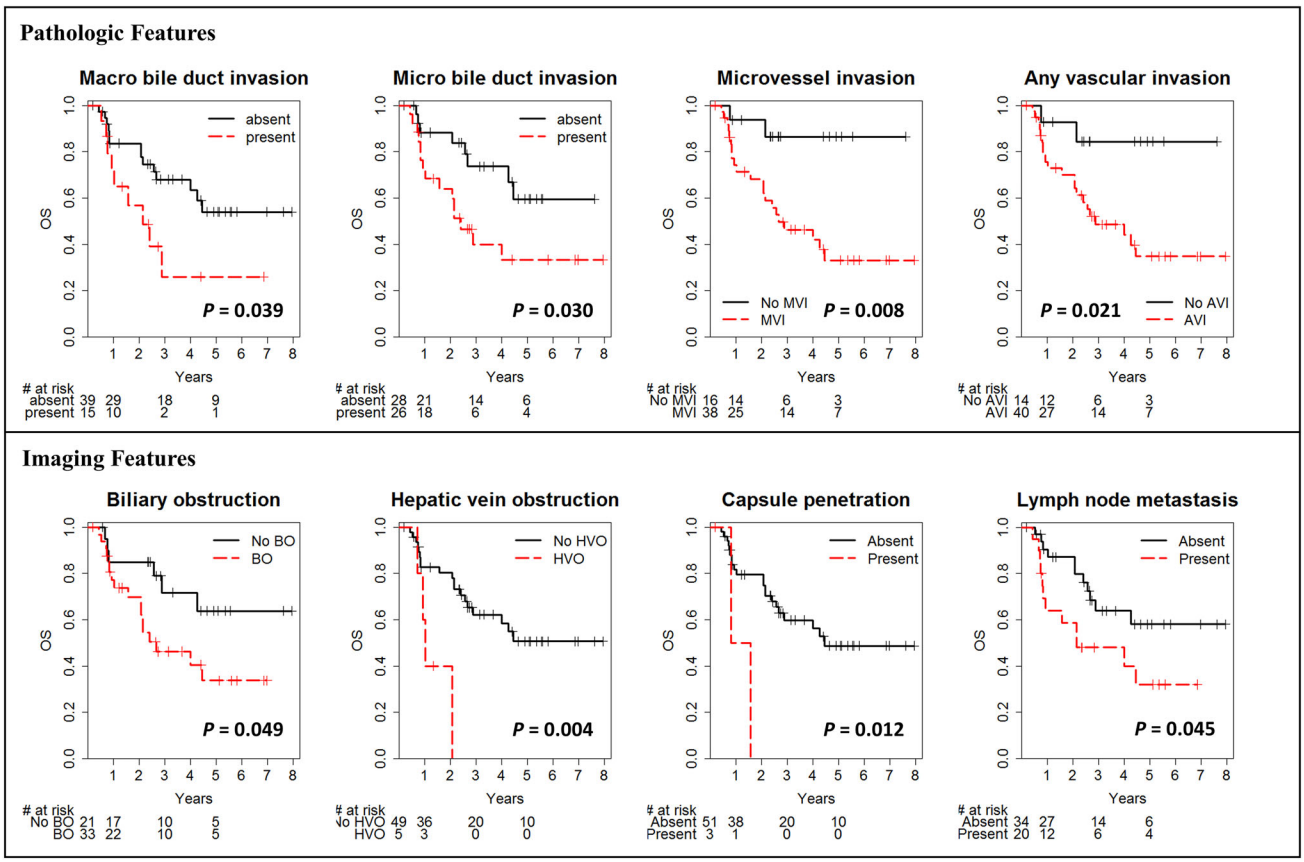

Fig. 5. Kaplan–Meier curves for OS in patients with intrahepatic mass-forming cholangiocarcinoma exhibiting different pathological and imaging features. OS is significantly poorer for patients with macroscopic or microscopic bile duct invasion, MVI, or AVI than for those without these features in pathological examination. In addition, OS is significantly poorer for patients with BO, HVO, capsule penetration, or lymph node metastasis than for those without these features on magnetic resonance imaging. *P* values were calculated using log-rank tests. Continuous variables-tumor size and age—were not plotted. OS, overall survival; MVI, microvessel invasion; AVI, any vascular invasion; BO, biliary obstruction; HVO, hepatic vein obstruction; CP, capsule penetration.

Fig. 6. Magnetic resonance imaging findings for a representative case involving a 66 year-old man exhibiting mass-forming intrahepatic cholangiocarcinoma with middle hepatic vein obstruction (arrow). Axial fat-suppressed T1-weighted three-dimensional gradient-recalled echo images obtained during the **A** arterial phase, **B** portal venous phase, and **C** hepatobiliary phase. The tumor exhibited a poor prognosis and recurred 4 months after resection. The patient survived for 12 months.

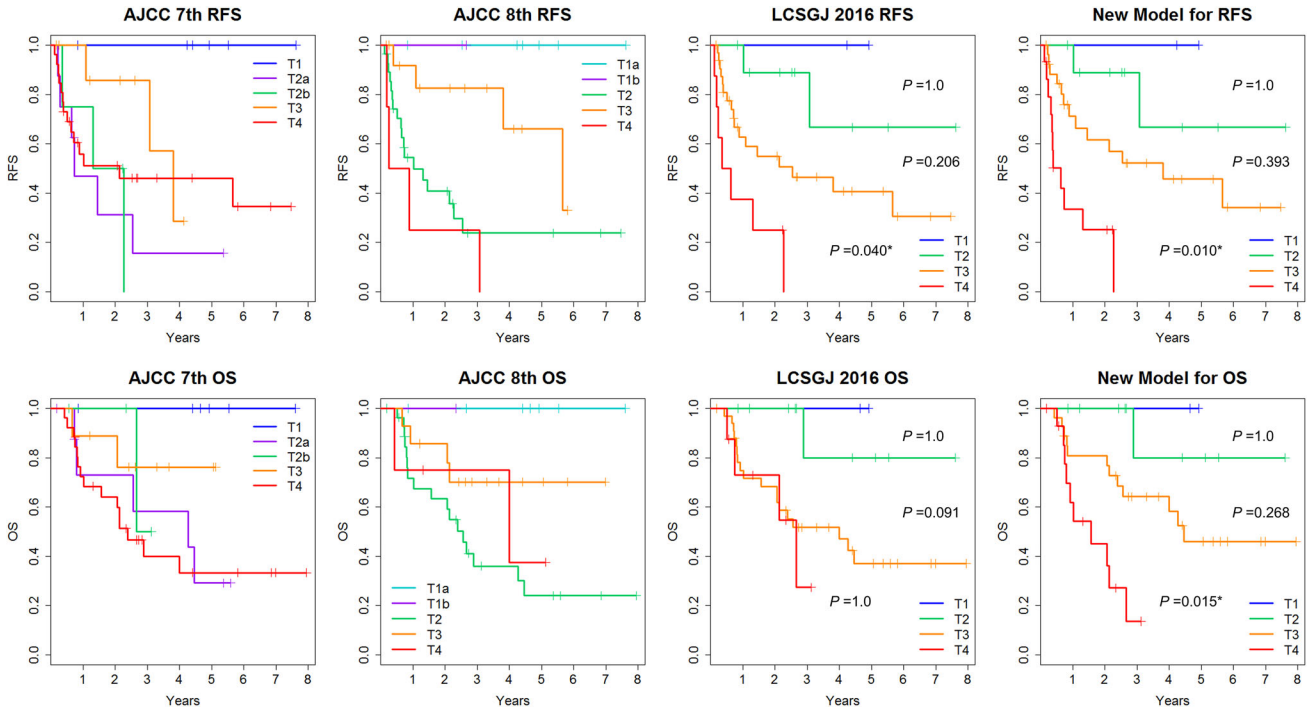

Fig. 7. Comparison of staging systems for intrahepatic cholangiocarcinoma based on the stratification of RFS and OS curves according to the tumor classification. Survival curves are not shown in the T-stage order in the AJCC 7th and 8th editions. LCSGJ shows survival curves in the T-stage order, although the distinction between stages T3 and T4 with regard to OS is inadequate. The new model shows the survival curves in the right order, with adequate distinction between stages. AJCC 8th, International Union Against Cancer/American Joint Committee on Cancer classification, 8th edition; LCSGJ 2016, recent staging system of the Liver Cancer Study Group of Japan (2016); RFS, recurrence-free survival; OS, overall survival.

system may improve prediction of the post-operative prognosis of IMCC.

Compliance with ethical standards

Funding Nothing.

Conflict of interest The authors declare that they have no conflict of interest.

References

1. Soyer P, Bluemke D, Reichle R, et al. (1995) Imaging of intrahepatic cholangiocarcinoma: 1. Peripheral cholangiocarcinoma. AJR. Am J Roentgenol 165(6):1427–1431
2. Morimoto Y, et al. (2003) Long-term survival and prognostic factors in the surgical treatment for intrahepatic cholangiocarcinoma. J Hepato Biliary Pancreat Surg 10(6):432–440
3. Hyder O, et al. (2014) A nomogram to predict long-term survival after resection for intrahepatic cholangiocarcinoma: an Eastern and Western experience. JAMA Surg 149(5):432–438. https://doi.org/10.1001/jamasurg.2013.5168
4. Sakamoto Y, et al. (2016) Proposal of a new staging system for intrahepatic cholangiocarcinoma: analysis of surgical patients from a nationwide survey of the Liver Cancer Study Group of Japan. Cancer 122(1):61–70. https://doi.org/10.1002/cncr.29686
5. Okabayashi T, Yamamoto J, Kosuge T, et al. (2001) A new staging system for mass-forming intrahepatic cholangiocarcinoma: analysis of preoperative and postoperative variables. Cancer 92(9):2374–2383
6. Edge SB, American Joint Committee on Cancer (2010) *AJCC cancer staging manual*, 7th edn. New York: Springer
7. Amin MB, et al. (2017) *AJCC Cancer Staging Manual*, 8th edn. New York: Springer
8. Fujita N, et al. (2017) Mass-forming intrahepatic cholangiocarcinoma: Enhancement patterns in the arterial phase of dynamic hepatic CT-correlation with clinicopathological findings. Eur Radiol 27(2):498–506. https://doi.org/10.1007/s00330-016-4386-3
9. Nanashima A, et al. (2013) Intrahepatic cholangiocarcinoma: relationship between tumor imaging enhancement by measuring attenuation and clinicopathologic characteristics. Abdom Imaging 38(4):785–792. https://doi.org/10.1007/s00261-012-9974-3
10. Turkoglu MA, et al. (2016) The favorable prognosis after operative resection of hypervascular intrahepatic cholangiocarcinoma: A clinicopathologic and immunohistochemical study. Surgery 160(3):683–690. https://doi.org/10.1016/j.surg.2016.03.020
11. Asayama Y, et al. (2006) Delayed-phase dynamic CT enhancement as a prognostic factor for mass-forming intrahepatic cholangiocarcinoma 1. Radiology 238(1):150–155
12. Horvat N, et al. (2018) Imaging features of hepatocellular carcinoma compared to intrahepatic cholangiocarcinoma and combined tumor on MRI using liver imaging and data system (LI-RADS) version 2014. Abdom Radiol 43(1):169–178. https://doi.org/10.1007/s00261-017-1261-x
13. Koh J, et al. (2016) Intrahepatic mass-forming cholangiocarcinoma: prognostic value of preoperative gadoxetic acid-enhanced MRI. Eur Radiol 26(2):407–416. https://doi.org/10.1007/s00330-015-3846-5
14. Chong YS, Kim YK, Lee MW, et al. (2012) Differentiating mass-forming intrahepatic cholangiocarcinoma from atypical hepatocellular carcinoma using gadoxetic acid-enhanced MRI. Clin Radiol 67(8):766–773. https://doi.org/10.1016/j.crad.2012.01.004
15. Lee J, Kim SH, Kang TW, et al. (2016) Mass-forming intrahepatic cholangiocarcinoma: diffusion-weighted imaging as a preoperative

prognostic marker. Radiology 281(1):119–128. https://doi.org/10.1148/radiol.2016151781
16. Pandey A, et al. (2018) Unresectable intrahepatic cholangiocarcinoma: multiparametric MR imaging to predict patient survival. Radiology 288(1):109–117. https://doi.org/10.1148/radiol.2018171593
17. Cohen J (1968) Weighted kappa: nominal scale agreement provision for scaled disagreement or partial credit. Psychol Bull 70(4):213
18. Landis JR, Koch GG (1977) The measurement of observer agreement for categorical data. Biometrics 33(1):159–174
19. Yamasaki S (2003) Intrahepatic cholangiocarcinoma: macroscopic type and stage classification. J Hepatobiliary Pancreat Surg 10(4):288–291. https://doi.org/10.1007/s00534-002-0732-8
20. Aherne EA, Pak LM, Goldman DA, et al. (2018) Intrahepatic cholangiocarcinoma: can imaging phenotypes predict survival and tumor genetics? Abdomin Radiol . https://doi.org/10.1007/s00261-018-1505-4
21. Gillies RJ, Kinahan PE, Hricak H (2015) Radiomics: images are more than pictures, they are data. Radiology 278(2):563–577